Chinese Chemical Letters 35 (2024) 109594

Contents lists available at ScienceDirect

Chinese Chemical Letters

journal homepage: www.elsevier.com/locate/cclet

Discovery of an enantiopure *N*-[2-hydroxy-3-phenyl piperazine propyl]-aromatic carboxamide derivative as highly selective $\alpha_{1D/1A}$-adrenoceptor antagonist and homology modelling

Junjun Huang[a,1,*], Ran Chen[a,1], Yajian Huang[b,1], Hang Zhang[c], Anran Zheng[a], Qing Xiao[a], Dan Wu[a], Ruxia Duan[a], Zhi Zhou[a], Fei He[c,*], Wei Yi[a,*]

[a] *The Fifth Affiliated Hospital, Guangzhou Municipal and Guangdong Provincial Key Laboratory of Molecular Target & Clinical Pharmacology, the NMPA and State Key Laboratory of Respiratory Disease, School of Pharmaceutical Sciences, Guangzhou Medical University, Guangzhou 511436, China*
[b] *Department of Pharmacy, The Third Affiliated Hospital of Guangzhou Medical University, Guangzhou 510150, China*
[c] *School of Traditional Chinese Medicine, Southern Medical University, Guangzhou 510515, China*

ARTICLE INFO

Article history:
Received 5 December 2023
Revised 26 January 2024
Accepted 29 January 2024
Available online 8 February 2024

Keywords:
Benign prostatic hyperplasia
α_1-AR antagonist
Phenylpiperazine
Homology modelling
Subtype selectivity

ABSTRACT

α_1-Adrenergic receptor (AR) blockers can be effective for the treatment of benign prostatic hyperplasia/lower urinary tract symptoms (BPH/LUTS), their usage is limited by cardiovascular-related side effects that are caused by the subtype nonselective nature or low selectivity of many current drugs. We previously reported that phenylpiperazine analogues with amide and propane linker were moderate $\alpha_{1D/1A}$ adrenoceptor antagonists and exhibited better anti-BPH effect than lead compound naftopidil (NAF) *in vivo*, however, with modest $\alpha_{1D/1A}$-subtype selectivity. Herein, we replaced propane moiety with 2-hydroxypropanol linker and synthesized twenty-seven racemic derivatives with modified aromatic and hetero aromatic groups. Of these new compounds, quinoline surrogate **17** exhibited extremely weak antagonistic affinity on α_{1B} in both cell-based calcium assay and tissue-based functional assay, so that elicited significant $\alpha_{1A/1B}$ and $\alpha_{1D/1B}$ selectivity. Intriguingly, the *R* enantiomer of **17** preferentially displayed superior anti-BPH effect in rat model compared with ***S*-17**, supporting ligand regulates the receptor in a highly stereospecific manner. Finally, the computer-aided modelling research was also performed in order to deeply understand the unique binding mode of ***R*-17** in complex with α_{1A} and the subtype receptor selectivity for ***R*-17** was also rationalized in this study. Taken together, our work enriched the diversity of phenylpiperazines for the treatment of BPH/LUTS, and provided a basis for discovery of $\alpha_{1D/1A}$-selective ligands.

Benign prostatic hyperplasia (BPH) is an abnormal increase in the size of the prostate gland due to unregulated hyperplasia growth of both epithelial and stromal cells of the prostate in the transitional zone surrounding the urethra [1,2]. BPH is a frequent cause of lower urinary tract symptoms (LUTS) in men and is a common benign neoplasm particularly in ageing men, the prevalence of BPH apparent in around 50% of men who are above 50 years, and 90% who are above 80 years old [3]. BPH/LUTS causes problems with micturition, including increased frequency, due to outflow obstruction that has a dynamic component due to α_1-adrenoceptors mediated contraction of the bladder back, prostate and urethra [4].

α_1-Adrenergic receptors (ARs) belong to G protein coupled receptor (GPCR) superfamily and coupled with $G_{q/11}$ protein involving phospholipase C activation, followed by the increase of intracellular calcium levels. In the late 1980s, molecular biology studies identified three α_1-AR subtypes, classified as α_{1A}, α_{1B} and α_{1D} [5]. α_{1A} plays a dominant role in controlling human prostatic smooth muscle contraction. Many α_{1A}-AR subtype selective antagonists have since been discovered, including silodosin [6], however, α_{1A}-selective compounds have not been proven to be very effective in relieving LUTS, especially the symptom of irritation. Subsequent research discovered that α_{1D} was involved in the mediation of LUTS, and the blocking of α_{1D} relaxes the detrusor muscles of the bladder which prevents storage symptoms, thus, additional α_{1D} antagonism may be useful, particularly in prostatic hy-

* Corresponding authors.
E-mail addresses: huangjunjun1985@gzhmu.edu.cn (J. Huang), hefei8131@smu.edu.cn (F. He), yiwei@gzhmu.edu.cn (W. Yi).
[1] These authors contributed equally to this work.

https://doi.org/10.1016/j.cclet.2024.109594
1001-8417/

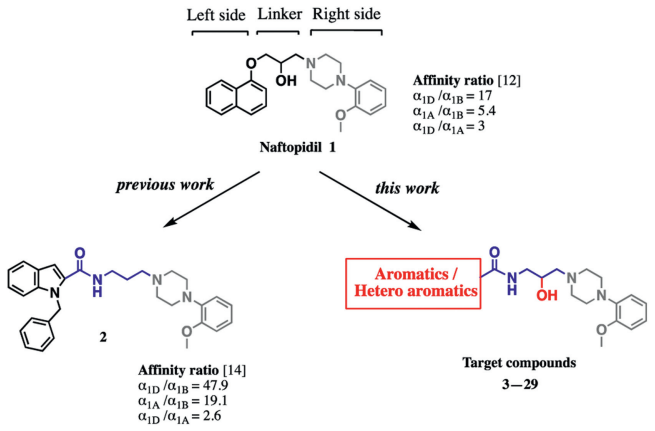

Scheme 1. Modification strategy of target compounds in present study.

perplasia [7,8]. On the other hand, antagonism of the α_{1B}-AR will lead to cardiovascular side effects, such as hypotension, as α_{1B} expressed predominantly in the heart and vascular smooth muscle [9,10]. Collectively, antagonists with better selectivity for α_{1A} and α_{1D} over α_{1B}-AR may alleviate the symptoms associated with BPH efficiently without causing significant cardiovascular side effects. Unfortunately, few ligands concomitantly recognize both α_{1A} and α_{1D} subtypes and rule out $\alpha_{1B,}$ such a lack of selectivity limits their administration *in vivo* and their therapeutic use [11].

Naftopidil (NAF, **1**) is a phenylpiperazine-based $\alpha_{1D/1A}$-AR antagonist used for treating BPH/LUTS in clinic [8]. NAF has approximately 3- and 17-fold higher potency for the α_{1D}-AR than for the α_{1A}- and α_{1B}-AR subtypes, respectively [12]. Our lab has engaged in the research of NAF and similar α_1 subtype blockers for years [13–17]. We previously synthesized phenylpiperazine related structures with amide and substituted indole ring (representative compound **2**, Scheme 1), which exhibited moderate $\alpha_{1D/1A}$-AR selectivity and satisfied anti-BPH activities *in vivo* [16,17], however, systematic structure–activity relationship (SAR) of this *o*-methoxyphenyl piperazine with carboxamide skeleton is still limited. Kuo *et al*. reported several structures of phthalimide-phenylpiperazines with 2-hydroxypropanol linker [18], whereas they only studied the substitution effect on phenyl ring which connected with phthalimide and without *in vivo* study yet.

Based on the recent resolved α_{1B} crystal structure bound with inverse agonist (+)-cyclazosin [19], a large proportion of aromatic residues were involved in binding pocket, and most of these amino acids were conserved in both α_{1A} and α_{1D} -ARs. This might also explained the proposed ligand pharmacophore model of α_1-ARs, in which one or two hydrophobic aromatic groups (HAR) were indispensable for maintaining activity [20,21]. Therefore, we herein replaced indole moiety of compound **2** with fused aromatics or various hetero cyclic rings (Scheme 1) in order to systematically study the effect of aromatics on the pharmacological profile. On the other hand, as we know that the degree of structure diversity in the left hand side was greater than that in the right hand side of molecule, we reserved *o*–methoxy phenylpiperazine group [11,22]. In addition, we also changed propane linkage into 2-hydroxypropanol to improve the flexibility of overall molecules. By utilizing above strategies, twenty-seven *N*-[2–hydroxy-3-phenylpiperazinepropyl]-aromatics carboxamide derivatives were designed and synthesized; highly selective and potent $\alpha_{1D/1A}$-subtype derivatives were expected. As a result, new surrogate **17** with quinoline ring was found to barely exhibit any affinity with α_{1B}-AR, and certainly performed a remarkable subtype selectivity towards α_{1A}- and α_{1D}-ARs. Chiral pharmacological behaviors of two enantiomers ***R*-17** and ***S*-17** were also investigated in rat BPH model, and *R*-configuration was found to behave as preferentially active enantiomer compared with its antipode. Solid SAR and computer-aided modelling study was also discussed in this research.

According to Scheme 1, mono-, double- and triple aromatic rings were considered as isosteres of naphthalene and were introduced to examine the influence of group size. Besides, aromatic rings with heteroatoms, such as *O*, *N* and *S* have quite different character and interaction potential with the binding site. Therefore, target compounds **3**–**29** were designed and shown in Scheme 2 [18]. Epoxide I was formed by substitution reaction with epichlorohydrin, followed by ring opening reaction with *o*–methoxy phenyl piperazine in 2-propanol to yield intermediate **II**. Intermediate **II** was then converted into prime amine **III** by deprotecting the phthalimide groups with hydrazine hydrate. The amine **III** was then coupled with various carboxylic acids using hexafluorophosphate azabenzotriazole tetramethyl uronium (HATU) to give the desired products **3**–**29**.

All target compounds were evaluated for their biological activities toward α_{1A}-AR using calcium mobilization assays [9,10]. The initial screening was carried out at a concentration of 10 μmol/L for each compound, and most of compounds displayed 90%–100% inhibition, so they were all further evaluated for their half-maximal inhibitory concentration (IC_{50}) values toward α_{1A}-AR (Table 1). Among all compounds, mono-ring substitution **3** and **4** showed the worst inhibitory activity (IC_{50} > 300 nmol/L). Indole substitution analogues **5**–**9** exhibited moderate antagonistic activity (IC_{50} > 100 nmol/L), while indazole derivatives **10**–**13** displayed ten times higher potency than indole ring (IC_{50} = 27.50–73.77 nmol/L). 7-Azaindole **14** and imidazo[1,2-*a*]pyridine **15** also performed comparable potency to indazole. Analogues **16** and **17** owned very small structural differences, however, introduction of quinoline (compound **17**, IC_{50} = 24.82 nmol/L) improved ten-fold higher activity compared with isoquinoline analogue (IC_{50} = 267.4 nmol/L), indicating the significance of the substitution position of overall aromatic ring. The following quinoxaline derivative **18** remained the same activity (IC_{50} = 30.23 nmol/L), which also supported that 2-substitution was preferred for α_{1A} receptor recognition, as 6-substituted quinoxaline derivative **19** led to a sharp reduction in potency (IC_{50} = 146.3 nmol/L). The same trend could also be observed on 1,4-benzodioxane compounds **20** and **21** (IC_{50} = 31.07 nmol/L *vs.* 82.02 nmol/L). In case of triple ring analogues, 9-xanthene derivative **28** showed almost equal activity as compared with tamsulosin (IC_{50} = 3.537 nmol/L), however, 9-anthracene substitution **29** resulted in a 35-times decrease of activity (IC_{50} = 122.5 nmol/L).

Overall, the introduction of hetero atoms into aromatic rings tend to improve the antagonistic affinity toward α_{1A}-AR, this might due to the hetero atoms behaved as hydrogen bond acceptor (HBA) group [21]. Meanwhile, multi-ring substitution exhibited satisfied antagonistic affinity compared with mono-aromatic derivatives, according to this, the pocket interacting this fragment might be characterized by the presence of more aromatic amino acid residues. A significant dependency on substituent position was also observed, which supported that distances and angles between pharmacophore features matter the magnitude of activity [23].

Next, top two promising α_{1A}- antagonist compounds (**17** and **28**, IC_{50} < 25 nmol/L) were selected to be further tested for their inhibitory activities toward α_{1B}- and α_{1D}-ARs. As shown in Table 2, quinoline analogue **17** behaved as $\alpha_{1A/1D}$- selective inhibitors, whereas compound **28** tend to display higher affinity toward α_{1A} and α_{1B}- subtypes than α_{1D}, probably due to the preference for recognition of bulky xanthene group by α_{1B}- receptor. Compound **17** aroused our great attention that exhibited very weak antagonistic affinity on α_{1B}-AR (IC_{50} = 7501 nmol/L), and salient subtype selectivity mainly toward α_{1A}- and to a minor extent on α_{1D}-

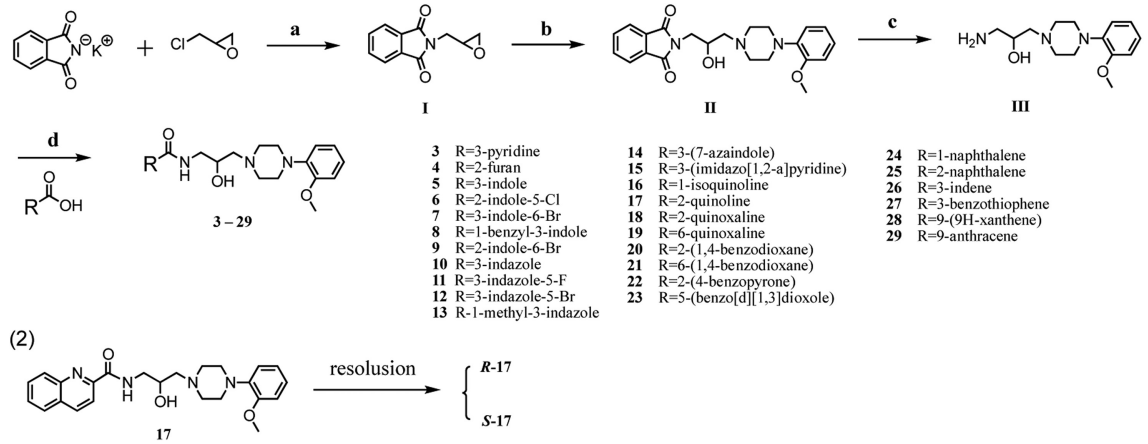

Scheme 2. (1) Synthesis of target compounds. Reagents and conditions: (a) reflux, 12 h, 86.7%; (b) *i*-PrOH, *o*–methoxy phenyl piperazine, reflux, 12 h, 89.9%; (c) $NH_2NH_2.H_2O$, EtOH, r.t., 89.05%; (d) HATU, DIPEA, CH_2Cl_2, N_2, r.t., 12 h, 51.1%–87.5%. (2) Resolution condition: CHIRALCEL OZ-H, 250 mm × 10 mm, 5 μm, Semi-Prep, MeOH:DEA = 1000:1 (v/v), UV 254 nm, 35 °C.

Table 1
Antagonist activities of all synthesized compounds for α_{1A}-AR.[a]

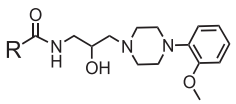

Comp.	R	IR (%)[b]	IC_{50} (nmol/L)	Comp.	R	IR (%)[b]	IC_{50} (nmol/L)	Comp.	R	IR (%)[b]	IC_{50} (nmol/L)
3		64	697.5 ± 51.2	**13**		99	73.77 ± 9.6	**23**		90	205.9 ± 46.9
4		81	376.2 ± 32.6	**14**		98	75.27 ± 4.5	**24**		100	68.82 ± 11.4
5		94	117.9 ± 9.2	**15**		95	81.62 ± 10.1	**25**		95	108.8 ± 8.7
6		90	360.2 ± 36.8	**16**		100	267.4 ± 42.1	**26**		100	192.9 ± 7.5
7		93	169.4 ± 40.6	**17**		99	24.82 ± 2.1	**27**		99	113.5 ± 5.4
8		93	204.4 ± 22.4	**18**		98	30.23 ± 5.7	**28**		92	3.537 ± 0.5
9		98	143.6 ± 14.5	**19**		96	146.3 ± 7.8	**29**		98	122.5 ± 21.4
10		99	27.50 ± 3.5	**20**		96	31.07 ± 2.4	Naftopidil		100	48.89 ± 3.5
11		100	40.67 ± 5.6	**21**		98	82.02 ± 5.3	Tamsulosin		100	2.565 ± 0.3
12		100	76.19 ± 10.3	**22**		95	103.3 ± 6.8	Silodosin		100	1.9 ± 0.1

[a] The initial screening was carried out at a concentration of 10 μmol/L for each compound, and IC_{50} values were measured for compounds that displayed >80% inhibition of α_{1A}-AR.

[b] IR represents inhibition ratio at a concentration of 10 μmol/L compound toward α_{1A}-AR.

Table 2
Subtype selectivity of compounds **17** and **28** using calcium assay.

Comp.	IC_{50} (nmol/L)			Selectivity		
	α_{1A}	α_{1B}	α_{1D}	α_{1D}/α_{1B}	α_{1A}/α_{1B}	α_{1A}/α_{1D}
17	24.82 ± 2.1	7501 ± 89.4	459.6 ± 30.2	16.32	302.22	18.52
28	3.537 ± 0.5	237.3 ± 25.5	817.5 ± 27.9	0.29	67.09	231.13
Tamsulosin	2.565 ± 0.3	7.506 ± 1.4	2.525 ± 1.8	2.93	2.97	0.98
Silodosin	1.9 ± 0.1	56.47 ± 3.5	6.106 ± 3.1	29.72	9.25	3.21

Table 3
Functional studies of compounds **17** and **28** on isolated rat tissues.

Comp.	pA_2 [a]			Affinity ratio [b]		
	Prostatic vas deferens (α_{1A})	Spleen (α_{1B})	Thoracic aorta (α_{1D})	α_{1D}/α_{1B}	α_{1A}/α_{1B}	α_{1D}/α_{1A}
17	7.63 ± 0.05	<5.5	8.62 ± 0.02	>1318.3	>134.9	9.77
28	7.75 ± 0.14	6.57 ± 0.03	8.43 ± 0.09	72.44	15.13	4.79
NAF	7.48 ± 0.30	6.75 ± 0.01	7.93 ± 0.13	15.1	5.4	2.8
Tamsulosin[c]	9.7 ± 0.10	8.9 ± 0.50	10.1 ± 0.10	5.0	1.4	3.5
Silodosin[d]	9.60 ± 0.05	7.15 ± 0.05	7.88 ± 0.55	5.4	281.8	0.02

[a] pA_2 values ± standard error of the mean (S.E.M.) ($n = 5–8$) were calculated from Schild plots, pA_2 is the positive value of the line intercept derived through plotting log(Dr-1) *vs.* log[antagonist].
[b] Antilog of ΔpA_2.
[c] Data from the previous report [23].
[d] Data from the previous report [6].

AR ($\alpha_{1A}/\alpha_{1B} = 302.22$, $\alpha_{1D}/\alpha_{1B} = 16.32$), exceeding reference drugs. Therefore, rat tissue based functional assay will be carried out to ensure their activity and selectivity.

The antagonistic effects of compound **17** and **28** on Sprague-Dawley rat prostatic vas deferens (α_{1A}), spleen (α_{1B}), and thoracic aorta (α_{1D}) were characterized to assess the sub-receptor selectivity of the compounds (Table 3). NAF mainly displays selectivity for α_{1D}- and, to a minor extent, for α_{1A}- with respect to α_{1B} -AR. Tamsulosin is a high affinity antagonist at functional α_1-ARs with a selectivity $\alpha_{1D} \geq \alpha_{1A} > \alpha_{1B}$ [24]. Silodosin is significantly more selective for α_{1A} abundant prostate tissue compared with other α_1-AR subtypes [6]. The inhibitory activity toward α_{1A}-AR of compound **17** and **28** was comparable to that of NAF, while, they improved the antagonistic activities on α_{1D} -AR ($pA_2 > 8$ *vs.* 7.93 of NAF). Both of these testing molecules displayed similar pA_2 values on α_{1A}- ($7.5 < pA_2 < 8$) or α_{1D}-ARs ($8 < pA_2 < 9$) and much higher subtype selectivity toward α_{1A}- and α_{1D}- ARs than reference drugs. We noted that the antagonist affinities toward α_{1A}- and α_{1D} in tissue-based functional assay diverged from cell-based calcium assay (Table 2), representing different trends, as testing compounds mainly blocked α_{1A} in calcium assay while they exhibited stronger inhibition on α_{1D} in tissue-based assay. This phenomenon might due to two different assessment systems between a recombinant receptor in cells and a native receptor in animal tissues [25,26]. With respect to α_{1B}, it is worth noting that compound **17** almost lost affinity on α_{1B} -AR ($pA_2 < 5.5$), which is consistent with the result of calcium assay, indicating that **17** might be a promising candidate for the treatment of BPH with high subtype selectivity.

Given the robust potential of compound **17** as a highly selective $\alpha_{1A/1D}$-antagonist, we further evaluated the anti-BPH effects of **17** in estrogen/androgen (E/T)-induced rat BPH model *in vivo*. The animal use and care protocols were reviewed and approved by the Ethics Committee of Guangzhou Medical University (approval number GY2022-208). Considering one chiral center was involved in the structure of **17**, two enantiomers might exert different pharmacological activities, therefore, ***R*-17** and ***S*-17** were separated by preparative HPLC using chiral column. The absolute configurations were identified by Mosher ester analysis (Figs. S1–S3 in Supporting information).

In the BPH model group, the values of wet weight, wet weight index, volume and volume index of the rat prostate were significantly larger than those in the sham operated group (Table 4, $P < 0.001$). Positive drug NAF (10.0 mg/kg) exhibited moderate effects on inhibiting both wet weight and wet weight index but little impact on prostate volume reduction, which was consistent with previous results [13,16]. Low dose (LOW, 2.0 mg/kg) of both ***R*-17** and ***S*-17** could not inhibit the progress of BPH, however, the situation was quite different when high dose (HIG, 5.0 mg/kg) administrated: ***R*-17** clearly decreased the wet weight index and volume index of hyperplastic prostate ($P < 0.001$), while ***S*-17** performed negligible effect on hyperplastic prostate.

The optical microscopy observations of hematoxylin–eosin-stained samples were compared, as shown in Fig. 1a. The sham operated group maintained the size and shape of the acinar gland well without atrophy. In the BPH model group, the glandular epithelium of prostate acini showed uneven hyperplasia; the contents of the lumen were increased, and the epithelial cells were markedly thickened. Administration of ***R*-17** and ***S*-17** displayed discrepancy: the prostatic acini apparently returned to normal with clear arrangement and uniform size in ***R*-17** HIG group, while ***S*-17** does not show obviously inhibitory activity. Quantitative analysis also supported that 5.0 mg/kg of ***R*-17** greatly suppressed the development of BPH with the minimum thickness of epithelium in rat prostate ($P < 0.001$ compared with model control group, $P < 0.001$ compared with ***S*-17** HIG group).

Smooth muscle alpha-actin (α-SMA) is a microfilament protein with contractile properties that is widely distributed in stromal smooth muscle in BPH human prostate [27]. In the BPH model, the acinus was surrounded with α-SMA positive smooth muscle layer compared with that in the sham operated group (Fig. 1b). Administration of ***R*-17** groups reduced thickness of the SMA-positive layer, and the most significant reduction was obtained at a high dose of ***R*-17**, indicating ***R*-17** could inhibit the extent of hyperplasia in stromal tissue in BPH to an extent. In addition, PCNA was used as a proliferation marker in rat prostate [28], and ***R*-17** HIG treatment obviously exhibited a decrease in PCNA expression (Fig. 1c, $P < 0.01$), while ***S*-17** did not show any effect. To estimate the effect of ***R*-17** and ***S*-17** on α_1-adrenoceptor subtypes *in vivo*, we analyzed the expression of α_{1A}, α_{1D}, and α_{1B} protein in prostate

Table 4
Effect of ***R*-17** and ***S*-17** on wet weight and volume of the rat prostate.

Group	Wet weight (mg)	Volume (cm^3)	Wet weight index (mg/g)	Volume index (cm^3/100 g)
Sham operated	810.2 ± 52.3[c]	0.82 ± 0.05[c]	2.65 ± 0.05[c]	0.22 ± 0.02[c]
BPH model	2116.8 ± 78.1	2.18 ± 0.07	8.30 ± 0.15	0.75 ± 0.04
NAF (10.0 mg/kg)	1630.1 ± 41.5[a]	2.01 ± 0.16	6.71 ± 0.22[b]	0.64 ± 0.04
***R*-17** LOW	1994.5 ± 32.1	1.97 ± 0.07	7.55 ± 0.18	0.62 ± 0.02
***R*-17** HIG	1218.1 ± 46.6[c]	1.80 ± 0.04[a]	5.22 ± 0.31[c]	0.55 ± 0.04[b]
***S*-17** LOW	1992.8 ± 33.8	1.98 ± 0.16	7.52 ± 0.10	0.65 ± 0.01
***S*-17** HIG	1875.3 ± 50.2[a]	1.91 ± 0.12	7.64 ± 0.14	0.60 ± 0.05

Values shown are the mean ± S.E.M. of 5 rats per group.
[a] $P < 0.05$, [b] $P < 0.01$, [c] $P < 0.001$ compared with BPH model group.

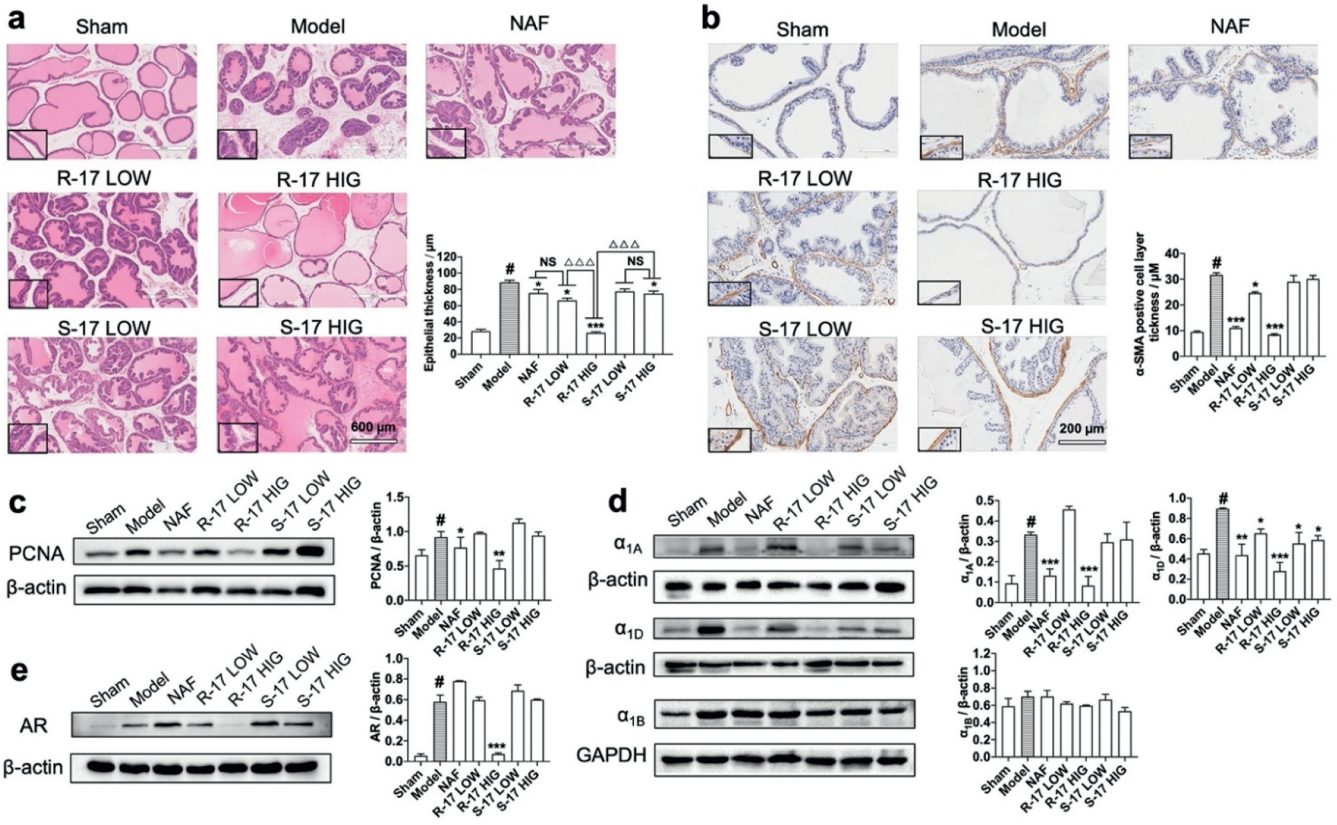

Fig. 1. *In vivo* BPH model investigation of ***R*-17** and ***S*-17**. (a) Histological changes of rat prostate tissue in various groups, including sham operated, model control, NAF (10.0 mg/kg), ***R*-17** LOW (2.0 mg/kg), ***R*-17** HIG (5.0 mg/kg), ***S*-17** LOW (2.0 mg/kg), ***S*-17** HIG (5.0 mg/kg); and quantitative analysis of epithelial thickness (μmol/L) in each group. (b) α-SMA expression of rat prostate tissue in each group and quantitative analysis of α-SMA positive cell layer thickness (μmol/L). (c) PCNA expression in the prostate tissue determined using Western blot. (d) Expression of α_{1A}-, α_{1B}- and α_{1D}-adrenoceptors and (e) AR of rat prostate tissue. Columns, mean values; error bars, S.E.M. ($n = 5$). Significance was determined using one-way ANOVA coupled with Tukey's multiple comparisons test. $^{\#}P < 0.05$ compared with the sham operated group. $^{*}P < 0.05$, $^{**}P < 0.01$, $^{***}P < 0.001$ compared with BPH model group. $^{\triangle\triangle\triangle}P < 0.001$. NS, no significance, $P > 0.05$.

tissue by Western blot analysis. As shown in Fig. 1d, the BPH group showed an increase in α_{1A} and α_{1D} expression compared with the sham-operated group ($P < 0.05$). The α_1-AR expression levels in the NAF-treated group were 0.13 ± 0.01 (α_{1A}, $P < 0.001$) and 0.43 ± 0.02 (α_{1D}, $P < 0.01$), which were lower than those in the BPH group. Low- and high-dose of ***S*-17** groups showed no effect on α_{1A} ($P > 0.05$), while exhibited decreased expression on α_{1D} ($P < 0.05$). Apparently, the high-dose ***R*-17** group produced remarkable reduction on both α_{1A} and α_{1D} ($P < 0.001$). Regarding of α_{1B}, no significant change was observed in all groups. We also executed Western blot on androgen receptor (AR) and only ***R*-17** HIG group strongly downregulated the AR expression in rat prostate tissue (Fig. 1e).

We are interested in the superior receptor selectivity of ***R*-17**, specifically, the unique behavior of low antagonistic affinity toward α_{1B}-AR. Although several subtype-selective ligand pharmacophore models and quantitative structure–activity relationship (QSAR) studies have been reported [21,23,29], this prediction greatly depend on structural diversity of training set compounds and model selection process. Herein, we would like to rationalize the receptor selectivity between α_{1A} and α_{1B}-AR by computer-aided modelling study.

Initially, the α_{1A} homology model (Fig. S4 in Supporting information) was constructed based on the sequence of α_{1B} (PDB id: 7B6W, resolution: 3.1 Å, co-crystallized with its inverse agonist (+)-cyclazosin) [19], the crystal structure of which was reported in 2022 and shares a relatively high BLAST identity of 63% with human α_{1A}. The rational binding pattern of compound ***R*-17** in complex with α_{1A} was carried out through multiple steps including homology modelling, induced-fit docking, molecular dynamics and clustering by Maestro (Schrödinger, LLC, New York, NY). The resulting five representative models which were generated after cluster-

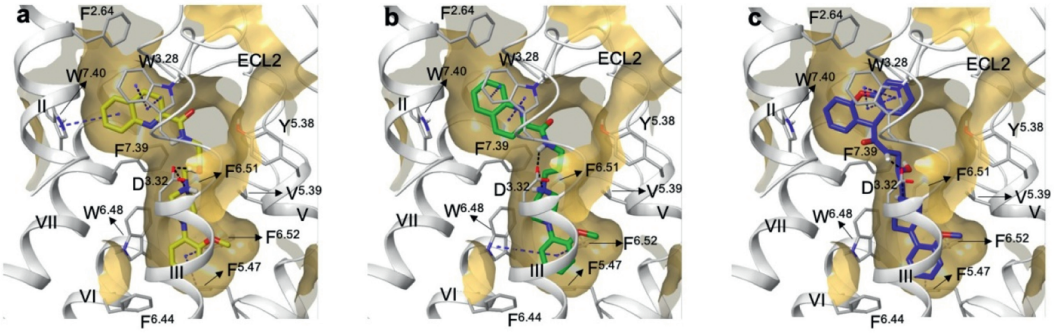

Fig. 2. ***R*-17** binding pocket (a) with human α_{1A} and ligand docking of **deoxy-17** (b) and **28** (c). Ligand was shown as thick tube in yellow (***R*-17**), green (**dexoy-17**), blue (**28**), respectively; helixes were shown as ribbons in silver color, amino acids were shown as thin tube in silver color; black dash line represent H bond or salt bridge, blue dash line represent aromatics including pi-pi stacking and pi-cation interaction.

ing based on ligand RMSD and SIFt (Structural interaction fingerprints) exhibited quite different ligand-binding conformations (Fig. S5 in Supporting information), and also different protein-ligand interaction profiles, therefore, 100 ns molecular dynamics (MD) was conducted for each model in order to examine the stability (Table S1 in Supporting information). Finally, Model 3 was selected to be a convincing binding pose shown in Fig. 2a and Fig. S6a (Supporting information).

Compound ***R*-17** was fitted nicely into the 7-shaped binding pocket of α_{1A}, which contains two aromatic (AR) centers on each side of ligand and one positive ionizable (PI) nitrogen of piperazine moiety (Fig. S6a). Two aromatic ring segments at both ends of ***R*-17** were shown: quinoline ring was positioned in a upper aromatic pocket, making aromatic-aromatic edge-to-face with W313$^{7.40}$ (the superscript refers to the Ballesteros-Weinstein numbering) and aromatic-aromatic stacking interaction with W102$^{3.28}$; on the other side, *o*-methoxyphenyl ring was positioned in a lower aromatic pocket, making pi-pi stacking with F289$^{6.52}$ and F193$^{5.47}$, and hydrophobic interaction with W285$^{6.48}$, F281$^{6.44}$, I114$^{3.40}$, T111$^{3.37}$ and C110$^{3.36}$. With respect to hydrophilic contacts, protonated N atom has salt bridge with D106$^{3.32}$, and this cation also interacted with electron-rich aromatic residue F312$^{7.39}$. Piperazine ring was also involved in hydrophobic interaction with V107$^{3.33}$, V185$^{5.39}$ and F288$^{6.51}$.

In this binding model, we noticed that the 2-hydroxypropanol linker displayed small extent of flexibility during MD simulation, as the orientation of *R*–hydroxy group behaves as a H bond donor (HBD) stably swing in the cavity between TM III and TM V, therefore, makes H-bond with D106$^{3.32}$ or Y184$^{5.38}$ alternatively (Fig. S6b in Supporting information). All of the above receptor-ligand interactions were stable during 200 ns MD simulation (Fig. S6c in Supporting information), and the ligand conformation and position does not show any significant fluctuation (Fig. S7 in Supporting information). In order to know the effect of this hydroxy group, we also synthesized the corresponding des–hydroxy compound (**deoxy-17**) and the resulting inhibitory activity toward α_{1A}-AR does not change ($IC_{50} = 20.26$ nmol/L for **deoxy-17** *vs.* 24.82 nmol/L for **17**). The docking pose of **deoxy-17** within α_{1A} was shown in Fig. 2b, in which binding position does not change regardless of the existence or absence of hydroxy group. This is to some extent consistent with previous study [19], in which des–hydroxy compounds also exhibited $\alpha_{1D/1A}$ subtype selectivity although with a lesser extent compared to hydroxy compounds, therefore, this hydroxy is not a necessary pharmacophore for α_{1A}-model.

The neighboring amide group was spatially proximal to extracellular loop 2 (ECL2) of α_{1A}, leading to interaction with water of membrane boundary (Fig. S8 in Supporting information). In addition, the *N* atom of quinoline also behaves as a H bond acceptor (HBA), making interaction with Y316$^{7.43}$ through water, the proposed pharmacophore features of ***R*-17** was shown in Fig. S6d (Supporting information). We then utilized this model to dock compound **28** which exhibited the best α_{1A} antagonistic activity ($IC_{50} = 3.537$ nmol/L). As expected, the xanthene ring with stronger conjugation system makes good pi-pi stacking interaction with W102$^{3.28}$, and could accommodate the upper aromatic pocket well (Fig. 2c), which in turn supported the feasibility of this binding model of α_{1A}.

With respect to α_{1B}, to our surprise, **deoxy-17** recovered the inhibitory activity toward α_{1B} ($IC_{50} = 329.8$ nmol/L for **deoxy-17** *vs.* 7501 nmol/L for **17**). We speculated that the fluctuation of flexible hydroxy group allowed compound **17** deviating from the pocket of α_{1B}. According to this hypothesis, we hence docked ***R*-17** and **deoxy-17** with α_{1B}, respectively. As expected, **deoxy-17** nicely accommodated in the α_{1B} (Fig. 3b), whereas the conformation of ***R*-17** completely distorted and nearly get out of this pocket, therefore easily lost salt bridge with D125$^{3.32}$ (Fig. 3a). It seems hydroxy

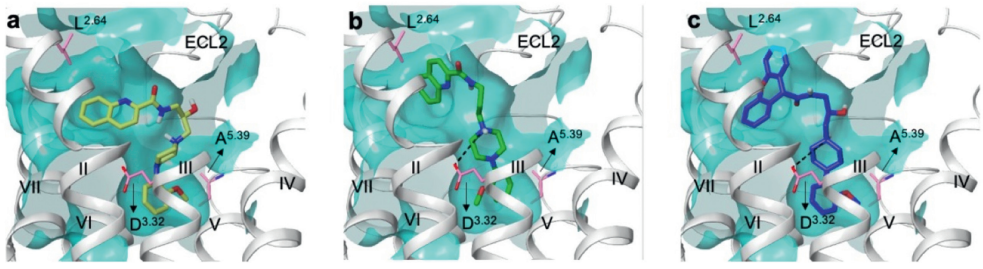

Fig. 3. Ligand docking of ***R*-17** (a), **deoxy-17** (b) and **28** (c) with human α_{1B}, respectively. Ligand was shown as thick tube in yellow (***R*-17**), green (**deoxy-17**), blue (**28**), respectively; helixes were shown as ribbons in silver color, amino acids were shown as thin tube in pink color; black dash line represent salt bridge.

group decided the selectivity between α_{1A}- and α_{1B}-AR, while this was not true. When another hydroxy compound **28** with comparative IC_{50} value ($IC_{50} = 237.3$ nmol/L for α_{1B}) docked with α_{1B}, it was shown that **28** fitted well and remain interaction with key residues of α_{1B} (Fig. 3c). All the above data suggested that the selectivity between α_{1A}-and α_{1B}-AR was influenced by both hydroxy group and upper aromatic moiety.

The flexible hydroxy group of ***R*-17** lead to complete detachment from α_{1B}, while it could stably make alternative interaction with D106 and Y184 in α_{1A}. However, this hydroxy group of **28** was not detrimental to α_{1B} and keep the moderate antagonistic affinity. Position 2.64 might contribute to ligand selectivity between α_{1A} and α_{1B}, since $L^{2.64}$ in α_{1B} allowed more space in this non-conserved cavity between TM3 and ECL2 compared to $F^{2.64}$ in α_{1A} (Fig. 2a of α_{1A} *vs.* Fig. 3a of α_{1B}). Thus, bulky xanthene ring of **28** might occupy this aromatic pocket of α_{1B} well in spite of the existence of flexible hydroxy group. Another speculation is small size of $A^{5.39}$ in α_{1B} (Fig. 3a) expanded the orthosteric pocket so that adversely affect the key interaction between NH^+ of **17** and $D^{3.32}$, while $V^{5.39}$ of α_{1A} makes appropriate distance in terms of hydrophobic interaction with piperazine ring and maintained the salt bridge with $D^{3.32}$ (Fig. 2a). Overall, small structural modification of ligand often makes subtype selectivity, our data supported to some extent that sequence variation within TM II showed to be a source of subtype selectivity for α_1-adrenergic ligands, however, more comprehensive study was needed.

In conclusion, we have identified a new, potent, and highly specific $\alpha_{1D/1A}$-AR antagonist, ***R*-17**, which presents a quinolinecarboxamide system and *o*-methyl phenylpiperazine scaffold connected by 2–hydroxy propanol linker. ***R*-17** displays very low antagonistic affinity toward α_{1B}, this super high selectivity of $\alpha_{1D/1A}$-ARs may contribute to the satisfied anti-BPH effect in the present study. We partly rationalize this subtype selectivity by proposing a convincing binding mode of ***R*-17** in complex with α_{1A} and compared with α_{1B} binding, several key residues were proposed. Our findings may guide the optimization of phenylpiperazines to elicit a selective interaction with the desired subtype, however, more detailed and profound research should be studied in near future.

Declaration of competing interest

The authors declare that they have no known competing financial interests or personal relationships that could have appeared to influence the work reported in this paper.

Acknowledgments

This work was supported by Natural Science Foundation of Guangdong Province (Nos. 2021A1515010101, 2021A1515011372, 2023A1515011895), National Natural Science Foundation of China (Nos. 21807017, 82273759, 32371529), Guangzhou Medical University Scientific Research Capacity Improvement Project (No. 02-410-2405104). We thank Professor Tomohiko Ohwada for technical support of calculation part.

Supplementary materials

Supplementary material associated with this article can be found, in the online version, at doi:10.1016/j.cclet.2024.109594.

References

[1] R.C. Langan, Urology 46 (2019) 223–232.
[2] S. Madersbacher, N. Sampson, Z. Culig, Gerontology 65 (2019) 458–464.
[3] B.M. Launer, K.T. McVary, W.A. Ricke, G.L. Lloyd, BJU Int. 127 (2021) 722–728.
[4] B. Chughtai, J.C. Forde, D.D.M. Thomas, et al., Nat. Rev. Dis. Primer 2 (2016) 16031.
[5] D.T. Price, D.A. Schwinn, J.W. Lomasney, et al., J. Urol. 150 (1993) 546–551.
[6] M. Yoshida, J. Kudoh, Y. Homma, et al., Clin. Interv. Aging 6 (2011) 161–172.
[7] J.R. Docherty, Eur. J. Pharmacol. 855 (2019) 305–320.
[8] G. Chiu, P.J. Connolly, S.A. Middleton, et al., Expert Opin. Ther. Pat. 18 (2008) 1351–1360.
[9] D. Guo, J. Li, H. Lin, et al., J. Med. Chem. 59 (2016) 9489–9502.
[10] F. Zhao, J. Li, Y. Chen, et al., J. Med. Chem. 59 (2016) 3826–3839.
[11] M. Pallavicini, R. Budriesi, L. Fumagalli, et al., J. Med. Chem. 49 (2006) 7140–7149.
[12] R. Takei, I. Ikegaki, K. Shibata, et al., Jpn. J. Pharmacol. 79 (1999) 447–454.
[13] J.J. Huang, Y. Cai, Y.Z. Yi, et al., Eur. J. Pharmacol. 791 (2016) 473–481.
[14] J. Huang, F. He, M. Huang, Eur. J. Med. Chem. 96 (2015) 83–91.
[15] J.J. Huang, Z.H. Zhang, F. He, et al., Bioorg. Med. Chem. Lett. 28 (2018) 547–551.
[16] Q. Xiao, Q.M. Liu, R.C. Jiang, et al., Front. Pharmacol. 11 (2021) 594038.
[17] Q. Liu, Q. Xiao, X. Zhu, et al., Eur. J. Pharmacol. 870 (2020) 172817.
[18] G.H. Kuo, C. Prouty, W.V. Murray, et al., J. Med. Chem. 43 (2000) 2183–2195.
[19] M. Deluigi, L. Morstein, M. Schuster, et al., Nat. Commun. 13 (2022) 382.
[20] H. Fang, M.Y. Li, L. Xia, Chin. Chem. Lett. 18 (2007) 41–44.
[21] E.S. Stoddart, S. Senadheera, I.J.A. MacDougall, et al., PLoS One 6 (2011) e19695.
[22] L. Fumagalli, M. Pallavicini, R. Budriesi, et al., J. Med. Chem. 56 (2013) 6402–6412.
[23] X. Zhao, M. Yuan, B. Huang, et al., J. Mol. Graph. Model. 29 (2010) 126–136.
[24] A.J. Noble, R. Chess-Williams, C. Couldwell, et al., Br. J. Pharmacol. 120 (1997) 231–238.
[25] C. Hosoda, A. Tanoue, M. Shibano, et al., Br. J. Pharmacol. 146 (2005) 456–466.
[26] S.W. Seto, S. Bexis, P.A. McCormick, et al., Eur. J. Pharmacol. 644 (2010) 113–119.
[27] M.T. Quiles, M.A. Arbós, A. Fraga, et al., Prostate 70 (2010) 1044–1053.
[28] N.G. Bahey, E.A.E. El-Drieny, J. Microsc. Ultrastruct. 3 (2015) 75–81.
[29] R. Barbaro, L. Betti, M. Botta, et al., J. Med. Chem. 44 (2001) 2118–2132.